AN AIRBORNE SAR EXPERIMENT FOR GROUND MOVING TARGET IDENTIFICATION

S. Suchandt[a], G. Palubinskas[a], H. Runge[a], M. Eineder[a], F. Meyer[a] and R. Scheiber[b]

[a] Remote Sensing Technology Institute, [b] Microwaves and Radar Institute,
German Aerospace Center (DLR) Oberpfaffenhofen, D-82234 Wessling, Germany

KEY WORDS: TerraSAR-X, Traffic Monitoring, Airborne SAR, Along Track Interferometry, Adapted SAR Processing

ABSTRACT:

With the launch of the advanced high resolution radar satellite TerraSAR-X in summer 2006 new possibilities open to demonstrate traffic monitoring from space. At the German Aerospace Center an automatic and operational traffic processor is developed for the TerraSAR-X ground segment. This comprises the detection of moving objects in Synthetic Aperture Radar (SAR) images, their correct assignment to the road network and the estimation of their velocities. An airborne SAR campaign with DLR's ESAR sensor was flown in an Along Track Interferometry (ATI) mode in April 2004 to investigate the effects of ground moving objects on SAR data and to acquire a data basis for algorithm development and validation for the traffic processor. Several vehicles with measured GPS tracks as well as vehicles on motorways with unknown velocities were imaged with the radar under different conditions. The paper provides an overview on the flight campaign and on the used experiment setups. Several data takes with different platform headings were acquired over a test site including controlled cars on a runway and over other test sites including motorways. The across track velocity was estimated by means of ATI phase. The measurements for experimental and road vehicles are presented, including comparison with GPS and optical reference data. To optimize the detectability of moving objects and to facilitate accurate speed measurements, adapted SAR processing approaches to compensate for energy losses because of a mismatched processed Doppler Centroid (due to across track motion) and because of defocused impulse responses (due to along track motion) were successfully applied to ESAR and SRTM data. Selected results and examples thereof are presented in the paper.

1. INTRODUCTION

Traffic plays a key role in economic as well as ecologic systems. Efficient transportation and travelling is an important factor in today's life. On the other hand, as the traffic density rapidly increases, it more and more influences our ecology. Air pollution, traffic jams and accidents have become serious problems. There exists a great demand for a large scaled acquisition of traffic information. Space borne synthetic aperture radar (SAR) technology could significantly contribute to this aim since it offers the possibility to image large areas under every weather condition. Moving objects cause several effects in SAR and interferometric SAR data and their measurement has been demonstrated for different SAR sensors, e.g. (Moreira 1995, Breit 2003, Gierull 2004). However, automatically detecting and measuring moving objects in SAR images, especially on an operational basis, is a complex and challenging task. With the launch of the advanced high resolution radar satellite TerraSAR-X in spring 2006 a door is opened for the demonstration of traffic monitoring with space borne SAR (Meyer 2004). Beside its various modes of operation and its high resolution of up to 1 m × 1 m, TerraSAR-X has been equipped with a dual receive antenna (DRA) mode, that enables the SAR antenna to be electronically split up in two parts in the along track direction upon receiving. This way along track interferometry (ATI) becomes possible, which is sensitive to moving objects. At DLR an automatic and operational traffic processor is developed for the TerraSAR-X ground segment. To study the different effects of moving objects in SAR images and to develop appropriate processing algorithms for their optimal detection and measurement, DLR has been conducting several airborne flight campaigns with its ESAR sensor. A first one in 2003 was dedicated to derive a radar backscatter model by imaging a cluster of stationary cars (Palubinskas 2004). In this paper the results from the 2nd flight campaign in April 2004 are presented, in which several moving vehicles in controlled and uncontrolled situations were imaged with the radar. The aims were to perform velocity measurements by means of SAR ATI and to experimentally quantify several effects of moving objects in SAR images.

1.1 SAR ATI Imaging of Moving Targets

The imaging geometry for the experiment is shown in Figure 1. Two SAR antennas A_1 and A_2 are spatially aligned in flight direction and are separated by the along track baseline B_{ATI}. As the platform moves forward with the velocity v_s, both antenna systems image the same area on ground with a temporal separation of B_{ATI}/v_s and under the look angle θ.

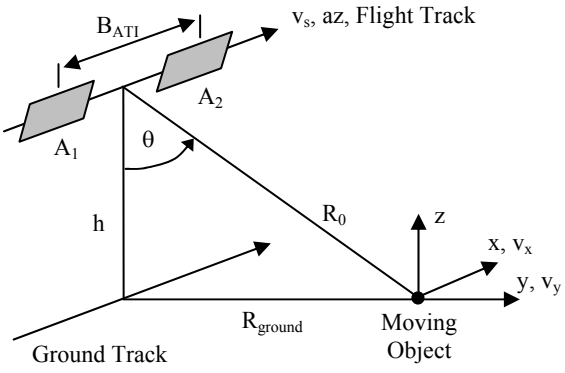

Figure 1: Imaging Geometry of SAR ATI System

Corresponding author: Steffen Suchandt, Email: steffen.suchandt@dlr.de, Phone: +49 8153 283011

Interferometric Phase
The interferometric phase of the system is given by

$$\phi_{ATI} = \left(\frac{4\pi \cdot B_{ATI} \cdot v_y \cdot \sin\theta}{\lambda \cdot v_s} \right) \bmod 2\pi \qquad (1),$$

with λ, the wavelength and v_y, the moving object ground range velocity. ϕ_{ATI} is sensitive to across track velocities but is zero for stationary objects or objects moving in the along track direction. It can be obtained only as a wrapped measure in the interval $[-\pi,\pi)$, thus higher across track velocities are ambiguously mapped into ϕ_{ATI}. The left part of Figure 2 shows an example of the ATI phase of moving objects.

Doppler Centroid Shifting and Azimuth Displacement Effect
When the sensor passes a target, its instantaneous Doppler frequency f_D linearly changes from positive to negative values at the Frequency Modulation (FM) rate. A standard SAR processor locates a target in azimuth where $f_D = f_{DC} = 0$. For an object with an across track velocity, an offset Δf_D is added to f_D. As a consequence, the moving object is focused with a wrong azimuth reference function. Due to Δf_D the target appears shifted in azimuth from its true position in the image by:

$$\Delta az = R_0 \frac{v_y \cdot \sin\theta}{v_s} \qquad (2).$$

An example of this effect can be seen in the right of Figure 2. During data acquisition, the signal is sampled in azimuth at the pulse repetition frequency (prf). Doppler frequencies > $|prf/2|$ appear as ambiguities in the base band. In the image, each target is represented by a main peak and by ambiguity peaks located $\pm prf^2/FM$ away from it in azimuth. For $|\Delta f_D| = 0$ the ambiguities are suppressed very well. As $|\Delta f_D|$ increases, azimuth focusing becomes less optimal for the main peak but more optimal for one of the ambiguities which will result in a reduced main peak and in an increased ambiguity peak energy. For $|\Delta f_D| = prf$ the ambiguity peak appears shifted to the true image azimuth position and with maximum energy, but the main peak appears shifted away from it by the same amount and strongly suppressed. Without further knowledge, the ambiguity peak can then not be distinguished from the main peak of a stationary object at the same position. Thus, also the displacement is subject to wrapping with an interval of

$$\Delta az_{amb} = R_0 \frac{prf \cdot \lambda}{2 \cdot v_s} \qquad (3).$$

Azimuth Defocusing Effect
The FM rate of a moving target with a velocity in azimuth direction v_x (positive in flight, negative in opposite direction) is

$$FM(v_x) = -\frac{2(v_s - v_x)^2}{\lambda R_0} \qquad (4).$$

In azimuth focusing the received signal of a target is usually compressed in the spectral domain with the matched filter

$$H(f, v_x) = \exp\left(j\pi \frac{1}{FM(v_x)} f^2\right) \qquad (5),$$

where f is the frequency. The nominal SAR azimuth focusing with $H(f,0)$, i.e. with the stationary world assumption, causes a smearing in azimuth direction when the target is moving in along-track direction, as shown in the right panel in Figure 2. Along-track motion changes the relative velocity of sensor and target resulting in a change of the FM rate and finally in a mismatch of the target's signal and the stationary world matched filter. The extent of this defocusing is directly proportional to the along-track velocity of the target.

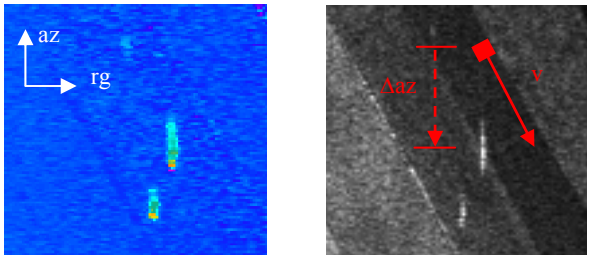

Figure 2: Examples of ATI phase alteration (left) and azimuth displacement and along track defocusing effect (right).

Defocusing of moving objects in SAR images may also be caused by accelerations, which are not treated here.

2. RESULTS FROM THE ESAR GMTI EXPERIMENT

2.1 Experiment Setup and Data Acquisition

ESAR Radar System
DLR's airborne experimental SAR sensor ESAR was used in the flight campaign for the acquisition of the radar data. This system has been in use for different applications and has been continuously improved and extended over a period of more than 16 years by now. It is operated on a Do-228 aircraft. Detailed descriptions of the sensor can be found in (Scheiber 1999). Table 1 lists the relevant ESAR system parameters for the SAR ATI experiment.

Parameter	Value
frequency band	X (9.6 GHz)
wavelength	0.311 m
range bandwidth	100 MHz
pulse repetition frequency	1000 Hz / channel
azimuth processing bandwidth	200 / 1000 Hz
along track baseline	0.87119 m
sensor forward velocity	88 m/s
altitude above ground	3940 m
incidence angle	20 – 60 deg
SLC pixel spacing (rg x az)	1.50 m x 0.087 m

Table 1: ESAR system parameters for experiment

Acquisition and Processing of Reference Data
To locate the vehicles in the radar images and to verify measurements, different reference data were recorded simultaneously with the SAR acquisition. Each vehicle was equipped with a GPS/DGPS receiver sampling the tracks with 1Hz. In order to have also reference data for vehicles on public roads, which were moving in uncontrolled situations, the sensor platform additionally carried an optical RMK-A camera, which took images at a sampling rate of about 0.3 Hz. These were processed to a resolution of 0.5 m and car positions and velocities were interactively extracted from sequences of images. The accuracy of this data was 2 m for the x,y-coordinates and about 5 km/h for the velocities. Details on the

processing of the optical data can be found in (Reinartz 2005). All reference data were interpolated.

Experiment Configuration and Data Takes

During the flight campaign 8 data takes were acquired as shown in Figure 3: 6 over the Oberpfaffenhofen airfield with controlled cars and 2 over motorway A95 near the cities of Munich and Wolfratshausen. As a by-product the latter data take was also used to demonstrate current measurements of the river Isar using SAR techniques.

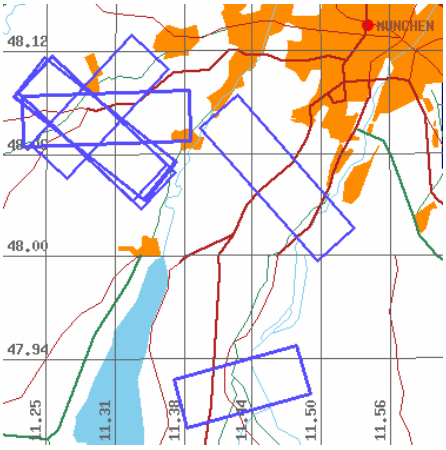

Figure 3: Acquired data takes

Figure 4 shows the configuration for the experiment at the Oberpfaffenhofen site. The platform heading (black) was varied from data take 1-6 to result in angles between the radar look direction (white) and the car heading of 0, 6, 45 and 90 degrees. This way, the influence of across track and along track velocity effects was controlled. There were slowly moving vehicles with velocities from 2-7 km/h (light blue) and fastly moving cars with velocities from 5-95 km/h (red). Some vehicles were equipped with radar reflectors to enhance visibility.

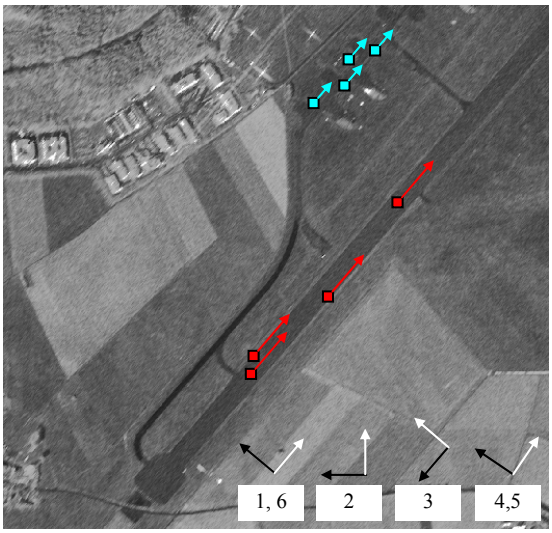

Figure 4: Configuration for Oberpfaffenhofen test site

2.2 Data Processing

At first the SAR raw data were focused with the standard ESAR processing software to motion compensated and co-registered pairs of single look complex (SLC) images. For the interferometric processing the GENESIS interferometry system which had already been used for ERS, SRTM and Envisat ASAR across track data was adapted for the ESAR ATI case. Interferometric processing included data import/conversion of ESAR data into the GENESIS format, geometry estimation, multilooking, interferogram generation, coherence estimation and interferometric phase correction. The latter step has to be applied because of so called channel imbalances. They are caused by small inequalities of the radar channels that can lead to offsets and trends in the ATI phase.

2.3 Across Track Velocity Measurement

2.3.1 Experiment Vehicles

The velocities of the experimental cars were estimated through the ATI phase. To enable a comparison with GPS reference data, the estimated across track velocities were geometrically projected back onto the GPS track. In cases of true velocity values exceeding the unambiguous phase range, the ATI phase was unwrapped. The measurements for data takes 1, 2, 5 and 6 are summarized in Table 2. The radar look direction for data take 3 was perpendicular to the car heading so that no across track component occurred. There are also no measurements for data take 4 due to a problem in reaching constant velocities with the imaged cars at the time of data acquisition. It was used to study acceleration effects instead.

Vehicle name	v_{GPS} [km/h]	ϕ [rad]	SCR [dB]	v_{ATI} [km/h]	dv [km/h]
Data Take 1					
V1	5.22	-1.66	9.95	5.36	0.14
V2	9.45	-2.92	17.1	9.46	0.01
V3	9.99	-2.93	18.88	9.19	-0.80
V4	2.15	-0.82	18.08	2.14	-0.01
V5	2.82	-0.63	11.02	1.68	-1.14
V6	4.82	-1.61	16.33	4.30	-0.52
V7	6.19	-2.25	20.01	5.96	-0.23
Data Take 2					
V1	4.96	-0.72	11.00	2.30	-2.66
V2	9.52	-1.92	14.64	8.88	-0.64
V3	10.65	-2.09	10.79	9.23	-1.42
V4	2.19	-0.54	13.00	2.05	-0.14
V5	2.45	-0.61	7.54	2.11	-0.34
V6	4.71	-1.10	18.41	4.31	-0.40
V7	6.33	-1.49	21.23	5.91	-0.42
Data Take 5					
V1	83.29	-0.41	11.47	78.40	-4.89
V2	10.41	3.13	12.56	10.10	-0.31
V4	2.27	-0.81	19.75	2.35	0.08
V5	3.79	-1.02	14.15	2.93	-0.86
V6	5.16	-1.71	14.68	4.66	-0.50
V7	6.24	-2.15	19.43	6.06	-0.18
Data Take 6					
V1	90.80	-2.82	9.53	83.71	-7.09
V2	10.01	3.11	16.79	9.94	-0.07
V3	2.16	-0.64	15.12	1.89	-0.27
V5	2.69	-1.01	15.98	2.84	0.15
V6	5.55	-1.70	17.15	4.58	-0.97
V7	6.34	-2.32	23.67	6.30	-0.04

Table 2: ATI velocity measurements for experimental cars. The Signal-to-Clutter Ratio (SCR) was determined from the backscatter of the cars and of the neighbouring areas.

Most of the ATI velocity measurements agreed very good with the reference data. In Figure 5 the relative error of the radar measurements from Table 2 is plotted against the true target

velocity. It can be seen, that there is evidence of increasing errors for low velocities.

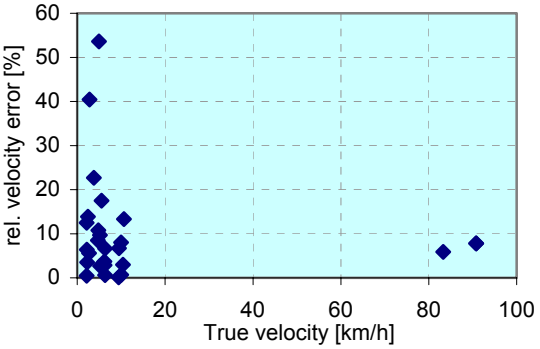

Figure 5: Relative error of ATI velocities for experimental cars

This can be explained by the fact that, for small Doppler shifts, the target spectrally lies in a region of high background clutter where the signal-to-clutter ratio is lower. This becomes more evident when the relative error is rearranged after the absolute base band Doppler shift (compare Figure 6).

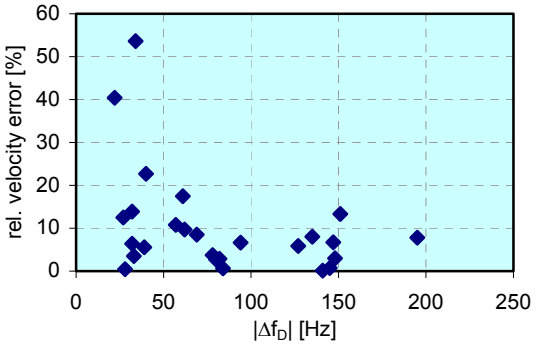

Figure 6: Relative error of ATI velocities for experimental cars as a function of (absolute) base band Doppler shift

2.3.2 Road Vehicles

The measurement for uncontrolled vehicles on public roads was carried out on data take 7. It included a motorway running mainly in the range direction of the radar. This way, defocusing effects due to along track velocities were avoided. The way the cars were evaluated is illustrated in Figure 7. At first the vehicle tracks, which had been extracted from sequences of optical images, were used to predict the time (or equivalently the azimuth image position) at which the radar must have seen them. Then the azimuth displacement was calculated from the LOS velocity using the imaging geometry and (2) and (3). The true and displaced positions of the car were mapped into the radar image afterwards (light blue squares with and without arrow). Points with a high peak energy at or near the predicted positions were selected for measurement. Assuming these points (red square) being moving objects, the across track velocity was estimated by measuring the ATI phase at these positions. With the obtained velocity, the (inverse) azimuth displacement was calculated to estimate the point's true origin (red square with arrow). NavTech™ road data had been automatically extracted from a database and mapped into the radar image (blue lines). Since ATI phase and azimuth displacement are ambiguous, this must be taken into account. In Figure 8 it is shown for the ESAR case, how ground range velocity, ATI phase and azimuth displacement are related.

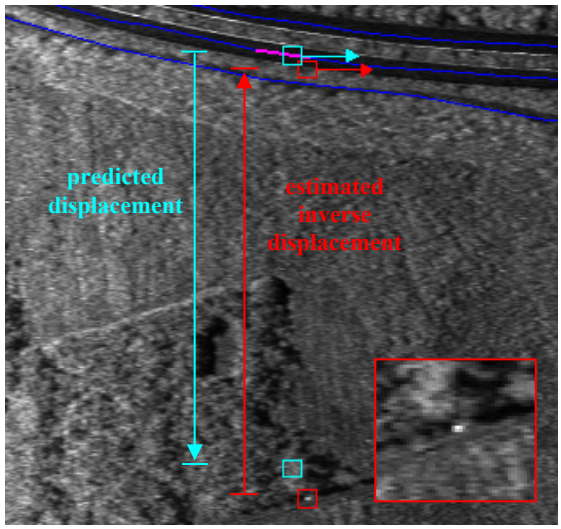

Figure 7: Evaluation of cars on public roads in SAR images

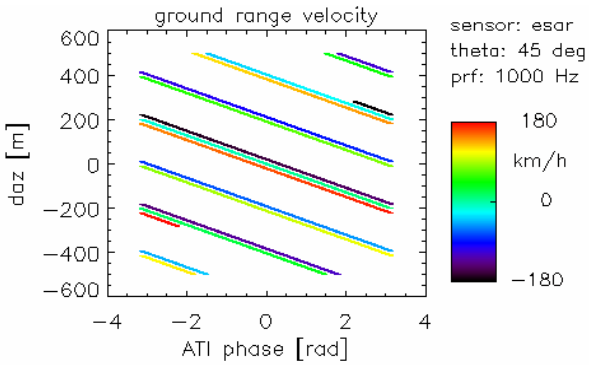

Figure 8: Ground range velocity for given ATI phase and azimuth displacement

If the points were moving targets, then there must be one phase ambiguity for which (I) the estimated displacement indicated a true origin on a road, (II) the estimated velocity (projected onto the closest street segment, shown in pink) was similar to that of one of the ground truth cars and (III) the true position of a car and the estimated origin were in good agreement. An exact agreement of both positions could not be obtained, since the estimates as well as the predictions from the reference data were subject to errors. While the range positions of the reference cars could be calculated quite accurate, the RMK velocity error of 5 km/h induced relatively high errors in the predicted azimuth displacement. Furthermore, as the cars on roads had not been equipped with reflectors, their SCR is significantly lower than that of the experimental cars, causing relatively high errors and biases in the velocity and inverse displacement estimations from ATI phase.

Table 3 summarizes the results for several points that met all conditions. Shown are the displacements and velocities for the RMK measurement in comparison with the estimations from the ATI phase and in addition with the ones obtained by exploiting the measurable displacements from the point targets to the road segments (taking into account Δaz ambiguities). The velocities estimated by means of the ATI phase and of the displacement method agree quite well with the RMK measurements. However, it must be stated that, though the motorway was highly populated with cars, not many were found in the radar image.

ATI				SAR		RMK	
SCR [dB]	ϕ [rad]	Δaz [m]	v_{ATI} [km/h]	Δaz [m]	v_{SAR} [km/h]	Δaz [m]	V_{RMK} [km/h]
9,9	-0,19	160	72	119	76	78	79
8,2	2,95	-238	77	-190	83	-189	82
10,9	0,05	-186	123	-209	125	-201	123
7,6	0,14	-150	82	-112	87	-93	88
16,5	0,04	-373	131	-384	132	-358	129
12,6	0,07	-181	129	-229	135	-237	136

Table 3: Estimations from radar data and reference measurements for cars in uncontrolled situations

In contrast to the cars in the runway experiment, they showed a significantly lower backscatter. The peak energy was further reduced by the Doppler shift effect. Consequently, to automatically detect cars in SAR images, there have to be applied adapted data processing strategies.

2.3.3 Multi-Doppler-Centroid-Processing

Moving objects with an across track velocity are focused with a wrong azimuth reference function in standard SAR processing. Besides the azimuth displacement, this results in a reduced energy of the base band peak and even in so called blind velocities (invisible moving objects), if the target spectrum, centred around f_D, is outside the processed bandwidth. A simulation was shown in (Breit 2003). The mismatched Doppler may also result in an increased energy of peak ambiguities. A way to accommodate for the Doppler shift of moving objects may be to process the SAR data with different Doppler Centroids, i.e. to centre the processed azimuth frequency band around f_D of the moving object. For the airborne SAR data this kind of processing leads to geometrically distorted images which are hard to interpret quantitatively. Data of the SRTM mission were taken instead to demonstrate the method. Due to the space borne SAR imaging geometry distortions of the stationary background do almost not occur. The selected data were acquired over the motorway A9 north of Munich, Germany. Figure 9 shows the amplitude (left) and the interferometric coherence (right) overlaid by a GPS track from the motorway. The SRTM interferometer configuration was such, that there was not only an across track but also an along track baseline of 7 m, so the instrument was sensitive also to across track motion. The strong point like alterations on both sides of the motorway in the coherence are caused by trucks that appear displaced due to an across track velocity component. There are several pairs of points, each of which appear at the same range position but displaced in opposite directions of the road. The points of a pair belong to the same object but at least one of it represents an azimuth ambiguity.

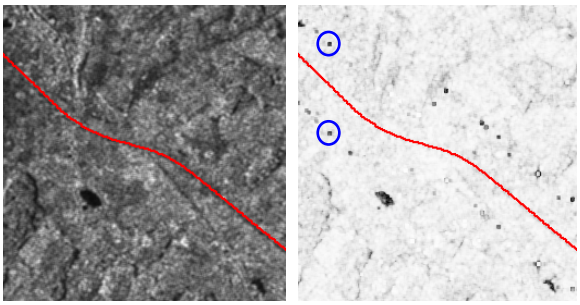

Figure 9: SRTM/X-SAR amplitude (left) and coherence (right) of German motorway A9

The energy of the moving object is distributed on two peaks. Multi-Doppler-Centroid processing was carried out for the pair marked in blue. The results can be seen in Figure 10. The five images are the processing results for five different Doppler Centroid values from -760 to 760 Hz (left to right). While the energy of one of the peaks is maximized as the Doppler frequency is varied, that of the other (ambiguity) peak is minimized. A second positive effect is that, when the peak is maximized, the background clutter power is minimized.

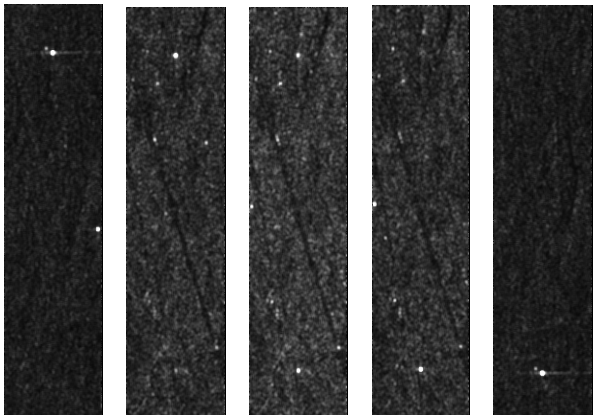

Figure 10: Multi-Doppler-Centroid processing of SRTM/X-SAR data.

2.4 Along Track Velocity Measurement

2.4.1 FM Rate Processing of E-SAR Data

In this section it will be shown how a moving object, that appears defocused due to an along-track velocity, can be sharpened, its peak energy can be increased and even its along track velocity can indirectly be derived.

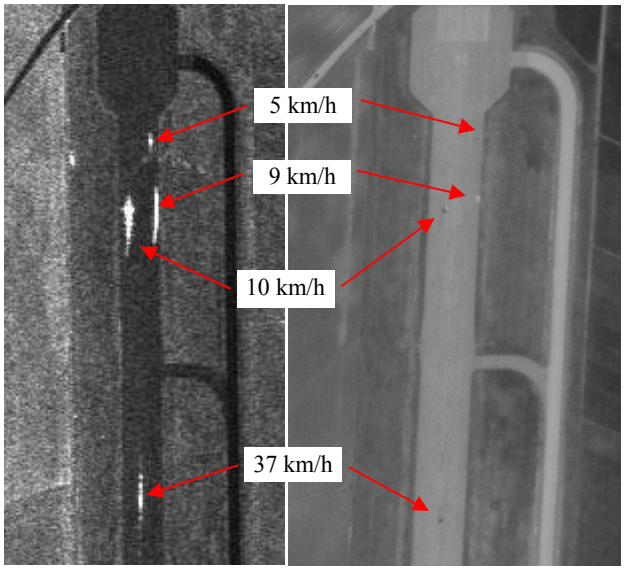

Figure 11: Test cars with different along-track velocities on the runway in a nominally processed radar image (left) and a reference optical image (right).

This is done by processing the SAR data with varying FM rates of the matched filter, thereby exploiting the specific behaviour of the target's signal through the FM rate space. Maximization of the peak energy is a necessary step to optimize the detection of moving targets and to reduce biases in the across-track

velocity determined from the ATI phase. In our E-SAR experiment the data were processed with a "stationary world assumption matched filter" *H(f,0)* in the beginning. After the standard processing, a corrective moving target post processing is performed with a matched filter $H(f,v_x)/H(f,0)$, where v_x runs over all possible along-track velocities for an analyzed scene. Figure 11 shows four test cars driving on the runway with different along-track velocities in a nominally processed radar image (left) and a reference optical image (right). The radar sensor flight direction was along the runway in this example. The radar signatures of the cars appear heavily defocused. The effect of the FM rate technique is demonstrated in Figure 12. For the car driving with an along-track velocity of 37 km/h it shows five radar images processed with different FM rates. The moving car is focused correctly when the matched filter with the FM rate for 37 km/h is used. This way, the along-track velocity component has been indirectly estimated!

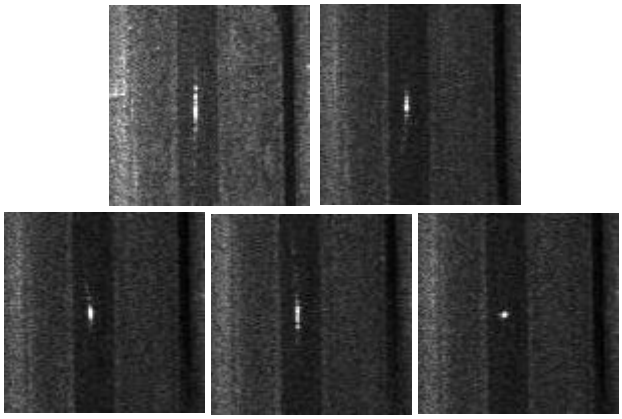

Figure 12: Five radar images of a car driving with an along-track velocity of 37 km/h processed with FM rates adapted for 0, 20, 37, 50 and 70 km/h (clockwise).

3. CONCLUSIONS

In the described airborne SAR ATI experiment the effects of moving objects were investigated and different vehicles in controlled and uncontrolled situations were imaged with the ESAR sensor. The experimental cars could easily be detected in the SAR images and their speed was estimated very accurately. The expected effects of displacement, defocusing and ATI phase alteration were clearly observed and quantified. The analysis of cars on public roads revealed, that the radar backscatter of these objects was very low, making detection and measurement more difficult. Nevertheless, the velocity and direction of several road cars could be estimated and was in good agreement with the reference data. However, to achieve high detection rates with an operational traffic processor for TerraSAR-X, adaptive SAR processing methods as proposed in this paper have to be applied. The stack like Multi-Doppler-Centroid and FM rate processing techniques have proven to be very effective, but may introduce a heavy computational load. A possible solution could be to process only image regions that most likely include moving object signatures. This calls for the incorporation of GIS data as demonstrated in section 2 with the NavTech^{TM} data base. Such a priori information enables to predict vehicle positions, i.e. to reduce the parameter space in which to search for moving objects in the data.

4. REFERENCES

Breit, H., Eineder, M., Holzner, J., Runge, H., Bamler, R., 2003. Traffic Monitoring using SRTM Along-Track Interferometry, Proc. of IEEE IGARSS 2003, 21-25 July, 2003, Toulouse, France.

Gierull, C.H., Sikaneta, I., 2004. Ground Moving Target Parameter Estimation For Two-Channel SAR, Proc. of EUSAR 2004, 25-27 May, 2004, Ulm, Germany, vol. 2, pp. 799-802.

Meyer, F., Hinz, S., 2004. The Feasibility of Traffic Monitoring with TerraSAR-X - Analyses and Consequences, Proc. of IEEE IGARSS 2004, 20-24 September, Anchorage, Alaska.

Moreira, Joao, R., Keydel, W., 1995. A New MTI SAR Approach Using the Reflectivity Displacement Method, IEEE Trans. Geoscience and Remote Sensing, vol. 33, No. 5, September 1995, pp. 1238-1244.

Palubinskas G., Runge H., Reinartz P., 2004: Radar signatures of road cars, Proc. of IEEE IGARSS, 20-24 September, 2004, Anchorage, Alaska, USA, vol. II, pp. 1498-1501.

Reinartz, P., Krauss, T., Pötzsch, M., Runge, M., 2005. Traffic Monitoring with serial images from airborne cameras, Proc. ISPRS High Resolution Mapping from Space 2005, Hannover, Germany.

Scheiber, R., Reigber, A., Ulbricht, A., Papathanassiou, K.P., Horn, R., Buckreuß, S., Moreira, A., 1999. Overview of Interferometric Data Acquisition and Processing Modes of the Experimental Airborne SAR System of DLR., Proc. of IEEE IGARSS 1999, Hamburg, Germany.

ACKNOWLEDGEMENTS

The authors would like to thank Ralf Horn from DLR's Microwave and Radar Institute for his efforts in planning the campaign flights and in carrying for the data acquisition.